
Critical Fluctuations and $1/f^\alpha$ -Activity of Neural Fields Involving Transmission Delays

A. HUTT*

Institute of Physics, Humboldt University of Berlin
Newtonstr. 15, 12489 Berlin, Germany

AND T.D. FRANK

Institute for Theoretical Physics, University of Münster
Wilhelm-Klemm-Str. 9, 48149 Münster, Germany

(Received 17 June, 2005; in final form 29 August, 2005)

This work studies the stability and the stochastic properties of neural activity evoked by external stimulation. The underlying nonlocal model describes the spatiotemporal response dynamics of neural populations involving both synaptic delay and axonal transmission delay. We show that the linear model recasts to a set of affine delay differential equations in spatial Fourier space. Besides a stability study for general kernels and general external stimulation, the power spectrum of evoked activity is derived analytically in the case of external Gaussian noise. Further applications to specific kernels reveal critical fluctuations at Hopf- and Turing bifurcations and allow the numerical detection of $1/f^\alpha$ -fluctuations near the stability threshold.

PACS numbers: 87.19.La, 05.40.Ca, 02.30.Ks, 05.70.Jk

1. Introduction

Random fluctuations have been reported in spatially-extended systems in biology, chemistry, and physics [1–3]. These fluctuations originate from thermal activity or unpredictable chaotic activity [4] and may yield novel effects as stochastic or coherence resonance [5] or noise-induced transitions [6]. In neural systems, background fluctuations are supposed to originate from spontaneous synaptic activity [7], while their spectral properties define the responsiveness of the neurons in the system [8]. In this context, several studies showed the importance of

*corresponding author; e-mail: Axel.Hutt@physik.hu-berlin.de

$1/f^\alpha$ -noise on both microscopic [9] and macroscopic level [10]. There are various effects of fluctuations on neural properties and we mention stochastic resonance enhancement measured in neocortical pyramidal cells [11] and modelled by induced $1/f$ -noise [12] and more general distributed noise sources [13]. In addition, noise may facilitate the detection of subthreshold neural activity [14, 15], which is known as stochastic resonance. The origins of long memory activity as $1/f^\alpha$ -noise is not fully understood yet. However, several mechanisms have been found [16, 17], for example the superposition of relaxation processes [18], noise in diffusion processes [19], clustering of signal pulses [20] and nonlinear processes with fractal characteristics [21]. Further Usher and Stemmler [9] explained $1/f$ -fluctuations in neural systems by pattern formation in neural populations subject to uncorrelated noise.

In addition to the spectral properties of fluctuations, some studies examined the change of their statistical properties while changing experimental conditions. For instance, Wallenstein et al. [22] examined electroencephalographic data obtained during a triggered motor coordination experiment, which reveals a phase transition in finger movements. Examinations of the occurring fluctuations revealed large fluctuation variances near the phase transition threshold both in the brain signals and the behavioural data. These critical fluctuations are well known from the theory of phase transitions. Several studies have modelled successfully this macroscopic phase transition and the corresponding critical fluctuations by mesoscopic population models [23–26]. Apart from these findings, further previous studies also indicate large-scale coherent phenomena in neural pathologies, which originate from mutual neural population activity. Examples are the hand tremor in Parkinson disease [27], epileptic seizures [28, 29] or hallucinations [30]. The latter in some cases exhibits a shift of the neural state to an instability by increased neuronal excitation [31]. Some studies explained visual hallucination patterns by stability loss in neural populations at bifurcation points [32, 33]. However, the mentioned neural models only treat a single time scale, namely the synaptic delay time. In contrast more recent approaches examine the stability of neural population fields involving constant delayed feedback [34, 29, 35, 36] or axonal transmission delay [37–41]. To our best knowledge, most of the latter stability studies neglect random fluctuations. However, these mesoscopic fluctuations may yield $1/f^\alpha$ -activity or explain macroscopic critical fluctuations as mentioned above and thus are necessary for realistic descriptions of neural systems.

Several previous studies examined the linear response of neural fields subject to external stimulation [26, 42, 44, 45]. However, some studies made special assumptions on the spatial connectivity kernels. For instance, several previous studies [42–44, 46] model the neural activity by damped nonlinear wave equations, i.e. partial differential equations, subject to external input. Since damped wave equations may be derived from integral–differential equations in the case of exponential kernels (cf. [23, 41]), those models implicate a special spatial connec-

tivity. That approach is reasonable for long-ranged cortico–cortical interactions, i.e. local inhibition and lateral excitation, and thus allows the theoretical explanation of macroscopic oscillatory behaviour. However, short-ranged interactions in specific cortical areas reveal different connectivity scheme, e.g. local excitation and lateral inhibition in visual cortex [47] or nonhomogeneous connectivity in prefrontal cortex [48]. In order to model neural activity by more general spatial connectivity schemes, it is necessary to choose a more general model approach.

In this context, several authors have shown the successful application of integral–differential equations to explain various phenomena in biology and neuroscience [32, 33, 37, 49, 50]. The present work follows this integral approach and studies the linear response of nonlocal neural fields to external input. It extends previous studies [24, 51, 52] by considering nonlocal interactions and involving transmission delay. The subsequent section motivates the neural field model and discusses briefly its properties. Section 3 shows a stability condition and the power spectrum of the field for general connectivity kernels. In the subsequent section, we examine specific synaptic kernels and find critical fluctuations near Hopf- and Turing instabilities. Finally, Section 5 studies the resulting power spectra numerically for excitatory diffusive fields for both infinite and finite transmission speeds. We find $1/f^\alpha$ -activity and long-term-memory activity near the stability threshold. The last section summarizes the obtained results and closes the work.

2. The field model

The present work treats activity in a spatially-extended field of neural populations [37, 53, 54, 46, 55–58]. In the following, we give a brief motivation of the discussed model, which has been examined in several previous studies [38, 39, 41, 57, 59, 60].

The model presumes neural activity, that is coarse-grained in space and time. The spatial coarse-graining originates from the treatment of macrocolumns, which represents the entity of neural ensembles [61]. Since these macrocolumns exhibit a diameter in the range of hundreds of micrometers and the modelled field discusses interaction on a scale of several centimeters, the model assumes continuity in space. The coarse-graining in time results from the temporal averaging of spike activity by slow synapses. This is reasonable, as the time scale of the spike-generating somatic membrane is much smaller than the synaptic time scale. Hence the mean spike activity evolves on the time scale of the synapses, i.e. typically $\sim 5\text{--}10$ ms [42].

Further, the model involves excitatory and inhibitory chemical synapses and neglects the transmission delay along dendritic structures. The synapses sum up all lateral contributions from other locations weighted by the synaptic connectivity kernels f_e and f_i for connections to excitatory and inhibitory synapses, respectively. These kernels represent probability density distribution of the corresponding synaptic connection and thus are normalized to unity. Here, we assume that the temporal changes of the synaptic coupling between neurons, e.g. by ha-

bituation or learning, evolve on a much larger time scale than the neural dynamics discussed. Furthermore the transmission speeds $v_{e,i}$ along axons are finite and thus yield the transmission delay $\Delta_{e,i} = |x - y|/v_{e,i}$ between two locations x and y . Essentially, chemical synapses respond to incoming spiking activity by temporal delay and, subsequently, the excitatory and inhibitory post-synaptic potentials $V_{e,i}$ at spatial position x and time t obey [38]

$$V_{e,i}(x, t) = \int_{-\infty}^t d\tau h_{e,i}(t - \tau) \left[\int_{\Gamma} dy f_{e,i}(x - y) S[V(y, \tau - \Delta_{e,i})] + E_{e,i}(x, \tau) \right]. \quad (1)$$

Here, $h_{e,i}(t)$ denote the impulse response functions of excitatory and inhibitory synapses, respectively, $V = V_e - V_i$ is the effective membrane potential and E_e and E_i represent the external excitatory and inhibitory inputs, respectively. The transfer function $S[V]$ originates from the statistical distribution of firing thresholds and exhibits a sigmoidal shape in the case of a unimodal threshold distribution. Eventually post-synaptic potentials $V_e - V_i$ sum up at the soma [62] and the final model equation for the somatic membrane potentials V reads

$$V(x, t) = \hat{I}_t \int_{\Gamma} dy \{ K_e(x - y) S[V(y, t - \Delta_e)] - K_i(x - y) S[V(y, t - \Delta_i)] \} + \hat{I}_t E(x, t) \quad (2)$$

with $h_{e,i}(t) = g_{e,i}h(t)$ and the synaptic gains $g_{e,i}$. In addition, it is

$$K_e = g_e f_e, \quad K_i = g_i f_i, \quad E = g_e E_e - g_i E_i$$

and \hat{I}_t represents the convolution operator acting on the test function $f(t)$ like

$$\hat{I}_t f(t) = \int_{-\infty}^t d\tau h(t - \tau) f(\tau).$$

Most cortical areas are a part of the neural modular network and receive external connections from other brain areas. Well-known examples are the cortico-thalamic subnetwork [63] studied in the context of sleep cycles and the projection from the lateral geniculate nucleus to the visual cortex. Hence, the neural field receives external input from cortical and subcortical areas. First we assume external excitatory input E_0 constant in space and time. Subsequently, the stationary constant field $V(x, t) = V_0$ obeys

$$V_0 = (g_e - g_i) S(V_0) + E_0.$$

Considering the external input E_0 as a control parameter, the corresponding bifurcation diagram exhibits either hysteresis with two stable and one unstable state or shows a single stable state V_0 [64].

Now, we consider small deviations $u(x, t) = V(x, t) - V_0 \ll V_0$ about the stationary solution V_0 and assume the additional external stimulus $s(x, t) \ll E_0$. Thus Eq. (2) reads

$$\begin{aligned}
 u(x, t) &= \hat{I}_t \gamma \int_{\Gamma} dy [K_e(x-y)u(y, t - \Delta_e) - K_i(x-y)u(y, t - \Delta_i)] \\
 &\quad + \hat{I}_t s(x, t). \tag{3}
 \end{aligned}$$

Here, $\gamma = \delta S / \delta V$ computed at $V = V_0$ depends implicitly on E_0 , while $\delta / \delta V$ denotes the functional derivative. Hence γ represents the control parameter for the linear case. The external stimulus $s(x, t)$ may correspond to a deterministic driving force, e.g. originating from sensoric perception. Alternatively, $s(x, t)$ may describe a fluctuating force acting on the neural field caused by synaptic fluctuations [7]. In fact, in Sect. 4 we will use Eq. (3) to study the stochastic evolution of $u(x, t)$ under the impact of a fluctuating force.

Since

$$\begin{aligned}
 K_{e,i}(x-y)u(y, t - \Delta_{e,i}) &= \int_{-\infty}^t d\tau K_{e,i}(x-y)\delta(t - \tau - \Delta_{e,i})u(y, \tau) \\
 &= \int_{-\infty}^t d\tau n_{e,i}(x-y, t - \tau)u(y, \tau)
 \end{aligned}$$

with $n_{e,i}(x, t) = K_{e,i}(x)\delta(t - \Delta_{e,i})$ and the delta-distribution $\delta(\cdot)$, the Fourier transform of Eq. (3) reads

$$\begin{aligned}
 \tilde{u}(k, t) &= \frac{1}{\sqrt{2\pi}} \int_{-\infty}^{+\infty} dx u(x, t) \exp(-ikx) \\
 &= \hat{I}_t \left[\gamma \sqrt{2\pi} \int_0^\infty d\tau \tilde{n}(k, \tau) \tilde{u}(k, t - \tau) + \tilde{s}(k, t) \right]. \tag{4}
 \end{aligned}$$

Here, \tilde{u} , \tilde{s} , and \tilde{n} represent the Fourier transforms of u , s , and $n = n_e - n_i$, respectively. Hence, in the linear regime the spatio-temporal dynamics of the neural field decouples into single modes in k -space, while the space-dependent propagation delay transforms to a distribution of constant delays.

Finally assuming symmetric kernels $K_{e,i}$ Eq. (4) reads

$$\begin{aligned}
 \tilde{u}(k, t) &= \hat{I}_t 2\gamma \int_0^\infty d\tau [v_e K_e(v_e \tau) \cos(kv_e \tau) - v_i K_i(v_i \tau) \cos(kv_i \tau)] \tilde{u}(k, t - \tau) \\
 &\quad + \hat{I}_t \tilde{s}(k, t). \tag{5}
 \end{aligned}$$

3. Stability analysis and power spectrum for general kernels

In this section, we set $v_e = v_i = v$ and use the abbreviation $K(x) = K_e(x) - K_i(x)$. Let us assume the inverse operator $\hat{I}_t^{-1} = \hat{L}(\partial / \partial t)$ exists, such that

$$\hat{L}(\partial / \partial t) h(t) = \delta(t), \quad t \geq 0,$$

while $h(t)$ is taken from (1). In addition, $h(t)$ is normalized to unity (cf. [42]). Then Eq. (5) becomes an affine delay differential equation (see e.g. [65]) with distributed delays

$$\hat{L}(\partial/\partial t)\tilde{u}(k, t) = 2v\gamma \int_0^\infty d\tau K(v\tau) \cos(kv\tau)\tilde{u}(k, t - \tau) + \tilde{s}(k, t). \quad (6)$$

Its general solution is

$$\tilde{u}(k, t) = \tilde{u}_h(k, t) + \int_{-\infty}^{+\infty} dt' G(k, t - t')s(k, t'), \quad (7)$$

where $\tilde{u}_h(k, t)$ represents the homogeneous solution of (6) and $G(k, t - t')$ represents the Greens function. Applying standard techniques in linear response theory, the Greens function is given by

$$G(k, t) = \frac{1}{2\pi} \int_{-\infty}^{+\infty} d\omega \frac{\exp(-i\omega t)}{L(-i\omega) - \bar{K}(k, i\omega)}, \quad (8)$$

where $\hat{L} \exp(-i\omega t) = L(-i\omega) \exp(-i\omega t)$ and

$$\bar{K}(k, i\omega) = 2v\gamma \int_0^\infty d\tau K(v\tau) \cos(kv\tau) \exp(i\omega\tau). \quad (9)$$

Extending the real domain of ω to the complex plane and applying the residue theorem, it is

$$G(k, t) = \Theta(t) \left[i \sum_{l=1}^m \text{Res}_l(\exp(-i\Omega_l t)) \right] = \Theta(t) \sum_{l=1}^m r_l(k) \exp(\lambda_l(k)t) \quad (10)$$

with the Heaviside function $\Theta(\cdot)$. Here, m denotes the number of complex roots $\Omega_l(k) \in \mathcal{C}$ of the denominator in Eq. (8), it is $\lambda_l(k) = -i\Omega_l(k)$ and Res_l denotes the residue of the numerator in Eq. (8) at root $\Omega_l(k)$. The constants $r_l \in \mathcal{C}$ are fixed by the corresponding residues. We remark that the vanishing denominator in Eq. (8) corresponds to the characteristic equation known from the theory of delayed differential equations.

In the case of large transmission speeds, $v \gg \omega$ yields

$$\bar{K}(k, i\omega) \approx \gamma \bar{K}_0(k) + i \frac{\omega}{v} \gamma \bar{K}_1(k), \quad (11)$$

$$\bar{K}_0(k) = 2 \int_0^\infty K(\tau) \cos(k\tau) d\tau, \quad \bar{K}_1(k) = 2 \int_0^\infty \tau K(\tau) \cos(k\tau) d\tau.$$

Here, the exponential in Eq. (9) has been Taylor-expanded up to the first order. In the case of infinite transmission speed the characteristic equation becomes $L(-i\Omega) = \gamma \bar{K}_0(k)$ and m is given by the order of \hat{L} .

Eventually, inserting Eq. (10) into Eq. (7), the solution of (6) reads

$$\tilde{u}(k, t) = \tilde{u}_h(k, t) + \sum_{l=1}^m r_l(k) \int_0^t dt' \exp(\lambda_l(k)(t - t')) \tilde{s}(k, t'),$$

assuming the stimulus onset at $t = 0$. If all roots are located in the lower complex plane, i.e. $\text{Im}(\Omega_l(k)) = \text{Re}(\lambda_l(k)) < 0$, Eq. (12) owns stable solutions for bounded deterministic stimuli and random fluctuations described by a Lévy process in the case of finite kernels [66].

As mentioned in the introduction, $1/f^\alpha$ -fluctuations have been found in neural populations. To detect this behaviour in our model, we briefly discuss the temporal power spectrum of the resulting field $u(x, t)$. The Fourier back transformation of (12) yields

$$u(x, t) = \tilde{u}_h(x, t) + \frac{1}{\sqrt{2\pi}} \sum_{l=1}^m \int_0^t dt' \int_{-\infty}^{\infty} \exp(\lambda_l(k)(t-t')) \tilde{s}(k, t') r_l(k) \exp(ikx) dk,$$

while $\tilde{u}_h(x, t)$ represents the homogeneous solution of Eq. (3). Now considering external uncorrelated Gaussian noise with

$$\langle \tilde{s}(k, t) \rangle = 0, \quad \langle \tilde{s}(k, t) \tilde{s}(k', t') \rangle = Q \delta(k - k') \delta(t - t'),$$

the autocorrelation function reads

$$C(t, \tau) = \langle u^*(x, t) u(x, \tau) \rangle = \frac{Q}{\pi} \sum_{l=1}^m \int_{-\infty}^{\infty} P_l(k) \exp(\lambda_l(k)|\tau - t|) dk \quad (12)$$

with

$$P_l(k) = - \sum_{j=1}^m \frac{r_j^*(k) r_l(k)}{\lambda_j^*(k) + \lambda_l(k)}.$$

Here, Q gives the overall strength of the fluctuation force, $\langle \cdot \rangle$ represents the ensemble average and $*$ denotes the complex conjugate. In addition, Eq. (12) assumes $t, \tau \rightarrow \infty$. Since the present work treats the neural resting state, the neural activity is stationary in time. Hence applying the Wiener–Khinchine theorem [67] the power spectrum reads

$$S^2(\omega) = \frac{-4Q}{(2\pi)^{3/2}} \sum_{l=1}^m \int_{-\infty}^{\infty} \frac{\lambda_l(k)}{\omega^2 + \lambda_l^2(k)} P_l(k) dk. \quad (13)$$

The function $P_l(k)$ gives the distribution of time scales $1/\lambda_l(k)$. Recalling the origins of $1/f^\alpha$ -activity [16], these multiple time scales may yield intermediate frequency regimes of $S^2(\omega) \sim 1/\omega^\alpha$ with $0 < \alpha < 2$. Subsequently, the presence of $1/f^\alpha$ -activity depends mainly on the synaptic connectivity kernels $K_{e,i}$ and on the relation of the synaptic to the axonal time scales defined by $h(t)$ and $v_{e,i}$, respectively. Closer investigations follow in Sect. 5 for specific kernels.

4. Stability and critical fluctuations for specific kernels

This section discusses the case of the exponential impulse response $h(t) = \exp(-t/\tau)/\tau$, i.e. $\hat{L}_t = \partial/(\tau\partial t) + 1$. The parameter τ represents the synaptic time scale. After re-scaling $t \rightarrow t/\tau$, we obtain $\hat{L}_t = \partial/\partial t + \tau$ and all time variables appear in relation to the synaptic time scale. Furthermore, we assume that the neural field is driven by a fluctuating force. That is, we put

$$s(x, t) = \sqrt{Q} \Gamma(x, t), \quad (14)$$

where $\Gamma(x, t)$ corresponds to a Gaussian distributed fluctuating force that is uncorrelated in space and time like

$$\langle \Gamma(k, t) \rangle = 0, \quad \langle \Gamma(k, t) \Gamma(k', t') \rangle = 2\delta(t - t')\delta(k - k').$$

The parameter Q represents the noise amplitude.

4.1. Hopf bifurcation

At first, we treat recurrent, i.e. local, excitatory connections, which play an important role in neural processing of somatic input signals. In addition, the inhibitory connections are lateral at a fixed distance. This case may occur in cortical areas, which participate in the thalamocortical projection system [68]. This system of axonal connections exhibit reciprocal, i.e. forth-and-back, projections from cortical areas to thalamic areas and thus introduce a constant temporal feedback delay. A previous study by Robinson et al. [43] showed that this feedback represents an important mechanism for generating global α -activity. Since there is poor knowledge in physiology about the distance distribution from the exiting to the terminating spatial location, we choose a single distance for simplicity. Subsequently, the kernels in (3) read

$$K_e(z) = \frac{g_e}{2\sqrt{D}} \exp(-|z|/\sqrt{D}), \quad K_i(z) = \frac{g_i}{2} \delta(|z| - |R|)$$

with $z = x - y$. Here, \sqrt{D} and R represent the excitatory and inhibitory spatial scale, respectively. For $\sqrt{D} \ll 1$ and $\sqrt{D}/v_e \ll 1$, the excitatory propagation delay is negligible yielding

$$\begin{aligned} & \int_{-\infty}^{+\infty} dy K_e(x - y)u(y, t - \Delta_e) \\ & \approx \left(\int_{-\infty}^{\infty} K(z)dz + \frac{1}{2} \int_{-\infty}^{\infty} K(z)z^2 dz \frac{\partial^2}{\partial x^2} \right) u(x, t) \\ & = g_e \left(1 + D \frac{\partial^2}{\partial x^2} \right) u(x, t). \end{aligned}$$

Hence, the local excitatory coupling is equivalent to diffusive coupling with diffusion coefficient D .

Following the analysis steps in Sect. 2 the corresponding delay differential equation in Fourier space becomes

$$\begin{aligned} \frac{\partial}{\partial t} \tilde{u}(k, t) &= [\gamma g_e(1 - Dk^2) - 1] \tilde{u}(k, t) \\ &\quad - \gamma g_i \cos(kR) \tilde{u}(k, t - t_0) + \sqrt{Q} \Gamma(k, t) \end{aligned} \quad (15)$$

with the delay $t_0 = R/v_i$. Introducing the parameters

$$a(k) = 1 - \gamma g_e + \gamma g_e Dk^2, \quad b(k) = \gamma g_i \cos(kR), \quad (16)$$

Eq. (15) can be written as

$$\frac{\partial}{\partial t} \tilde{u}(k, t) = -a(k)\tilde{u}(k, t) - b(k)\tilde{u}(k, t - t_0) + \sqrt{Q}\Gamma(k, t). \quad (17)$$

That is, we deal with a linear stochastic delay differential equation for the Fourier amplitudes $\tilde{u}(k, t)$ that involves k -dependent parameters. Let us discuss Eq. (15) in the context of the emergence of oscillatory behaviour. To this end, we first examine the behaviour of the spatially homogeneous Fourier mode with $k = 0$. We have $a(0) = 1 - \gamma g_e$ and $b(0) = \gamma g_i$. For $k = 0$ and $a(0) \geq b(0) > 0$ Eq. (17) describes a stable system both in the deterministic ($Q = 0$) [65, 69] and the stochastic case ($Q > 0$) [51, 52, 70–72]. Therefore, we assume that $b(0) > a(0) > 0$. Then, for $k = 0$ and $Q = 0$ the linear model (17) exhibits a stable (unstable) fixed point $\tilde{u}_{\text{st}}(0) = 0$ for delays t_0 smaller (larger) than the critical delay

$$t_{0,c} = \frac{1}{\Omega} \arccos\left(-\frac{a(0)}{b(0)}\right), \quad \Omega = \sqrt{(b(0))^2 - (a(0))^2}. \quad (18)$$

At $t_0 = t_{0,c}$ there is a Hopf bifurcation [65, 69] at frequency Ω . Likewise, for $k = 0$ and $Q > 0$ Eq. (17) exhibits stationary distributions for delays $t_0 < t_{0,c}$, whereas for delays $t_0 > t_{0,c}$ stationary distributions do not exist [51, 52, 70–72]. The stationary distributions for $t_0 < t_{0,c}$ correspond to Gaussian distributions with vanishing mean and variance σ^2 defined by

$$\sigma^2 = \frac{Q}{2} \frac{(1 + \Omega)^{-1} b(0) \sin(\Omega t_0)}{a(0) + b(0) \cos(\Omega t_0)}. \quad (19)$$

It is clear from Eq. (19) that σ^2 becomes infinite at the bifurcation point. Furthermore, from Eq. (17) it follows that the first moment $M_1 = \langle \tilde{u}(0, t) \rangle$ evolves like

$$\frac{d}{dt} M_1(t) = -a(0)M_1(t) - b(0)M_1(t - t_0). \quad (20)$$

Equation (20) can be treated just as Eq. (17) for $Q = 0$. That is, Eq. (20) describes a Hopf bifurcation and for $t_0 > t_{0,c}$ the first moment M_1 oscillates with a gradually increasing amplitude. Next, let us consider Fourier modes with nonvanishing k -values. To this end, we need to distinguish between two cases: $|k|R \leq \pi/2$ and $|k|R > \pi/2$. In the first case, we have $a(k) > a(0)$ and $b(k) < b(0)$. Consequently, if the homogeneous Fourier mode is stable, then all Fourier modes with $|k|R \leq \pi/2$ are stable. In the second case, we assume that the diffusion coefficient D satisfies the inequality $g_e D k^2 \geq g_i$ for $|k|R > \pi/2$, which implies that $a(k) > b(k)$ holds (e.g. one may choose $D = 4g_i R^2 / (g_e \pi^2)$). Then, the Fourier modes with $|k|R > \pi/2$ are stable as well.

Taking a neurophysiological point of view, it is of particular interest to study the impact of the control parameter γ (see Sect. 2). From Eq. (18) it follows that the critical parameter γ_c is given by

$$t_0 \sqrt{\gamma_c^2 g_i^2 - (1 - \gamma_c g_e)^2} = \cos\left(-\frac{1 - \gamma_c g_e}{\gamma_c g_i}\right). \quad (21)$$

In sum, for delays $t_0 < t_{0,c}$ or control parameters $\gamma < \gamma_c$ all Fourier modes described by Eq. (17) correspond to stable modes that have in the deterministic case stable fixed points at $\tilde{u}_{\text{st}}(k) = 0$ and exhibit in the stochastic case Gaussian stationary distributions with vanishing mean and variance

$$\sigma^2(k) = \frac{Q}{2} \frac{1 + w^{-1}(k)b(k) \sin(w(k)t_0)}{a(k) + b(k) \cos(w(k)t_0)}, \quad (22)$$

where $w(k)$ is defined by

$$w(k) = \sqrt{b^2(k) - a^2(k)} \quad (23)$$

(let us note that Eq. (22) holds even if w corresponds to an imaginary value [73]). As a result, the neural field is spatially homogeneous. For $t_0 \rightarrow t_{0,c}$ or $\gamma \rightarrow \gamma_c$ the variance of the amplitude of the homogeneous Fourier mode with $k = 0$ becomes infinite, whereas the variances of all other Fourier amplitudes are still finite, see also Fig. 1. In this sense the neural field exhibits critical fluctuations at the bifurcation point. If $t_0 = t_{0,c} + \epsilon$ or $\gamma = \gamma_c + \epsilon$ with ϵ positive and small, then the amplitude $\tilde{u}(0, t)$ and amplitudes $\tilde{u}(k, t)$ with small k -values become unstable

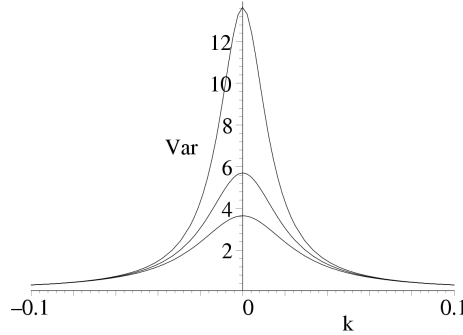


Fig. 1. Variance σ^2 as a function of k for several parameters of γ as computed from Eq. (22). For $\gamma \rightarrow \gamma_c$ the variance of the critical mode with $k_c = 0$ tends to infinity, whereas the variances of all other modes remain finite. Control parameters (from bottom-up): $\gamma = 1.00$, $\gamma = 1.02$, $\gamma = 1.04$. Other parameters: $t_0 = 1.0$, $g_e = 0.2$, $g_i = 2.0$, $Q = 1.0$, $R = 10$, $D = 4g_i R^2 / (g_e \pi^2)$ and $\gamma_c = 1.05$.

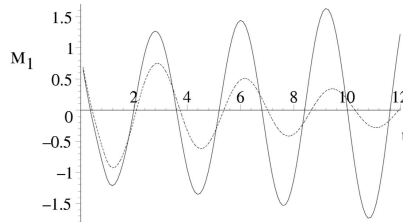


Fig. 2. Evolution of the first moment $M_1(t)$ of the critical mode $k_c = 0$ computed from Eq. (20) for two cases: $\gamma = 0.9 < \gamma_c$ (dashed line) and $\gamma = 1.1 > \gamma_c$ (solid line). Other parameters as in Fig. 1.

and the first moments $M_1(k, t) = \langle \tilde{u}(k, t) \rangle$ of these modes oscillate with gradually increasing amplitudes, see Fig. 2. Consequently, constant oscillations emerge in the neural field and we deal with critical fluctuations at the bifurcation point of constant waves.

4.2. Turing bifurcation

Now, we discuss the case of local excitation and lateral inhibition in intracortical fields. This Mexican-hat connection scheme is prominent in somato-sensory cortical areas, e.g. in the visual and auditory system. In this context, the spatial dimension represents a feature dimension. For instance, orientation selectivity of visual stimuli necessitates a Mexican-hat topology of the visual cortex, i.e. local excitation and lateral inhibition, while the orientation angle of the visual stimulus represents the feature variable [74, 75]. That is, we use [38]

$$K_e(x) = \frac{g_e}{2r_e} \exp(-|x|/r_e), \quad K_i(x) = \frac{g_i}{2r_i} \exp(-|x|/r_i),$$

where $r_{e,i}$ denote the excitatory and inhibitory spatial ranges with $r_e < r_i$. Using the previous re-scaled temporal operator $\hat{L}_t = \partial/\partial t + 1$ and $v_e = v_i = v$, Eq. (6) becomes

$$\begin{aligned} \frac{\partial}{\partial t} \tilde{u}(k, t) &= -\tilde{u}(k, t) \\ &+ v\gamma \int_0^\infty d\tau \left(\frac{g_e}{r_e} \exp(-v\tau/r_e) - \frac{g_i}{r_i} \exp(-v\tau/r_i) \right) \\ &\times \cos(kv\tau) \tilde{u}(k, t - \tau) + \sqrt{Q} \Gamma(k, t). \end{aligned} \tag{24}$$

The ansatz $\tilde{u}(k, t) = u_k \exp(\lambda t)$ yields the characteristic equation

$$\lambda + 1 = \gamma \left[g_e \frac{1 + \lambda r_e/v}{(1 + \lambda r_e/v)^2 + r_e^2 k^2} - g_i \frac{1 + \lambda r_i/v}{(1 + \lambda r_i/v)^2 + r_i^2 k^2} \right], \tag{25}$$

which corresponds to a polynomial of 5th order. The first moments $M_1(k, t) = \langle \tilde{u}(k, t) \rangle$ evolve like

$$\begin{aligned} \frac{\partial}{\partial t} M_1(k, t) &= -M_1(k, t) + v\gamma \int_0^\infty d\tau \left(\frac{g_e}{r_e} \exp(-v\tau/r_e) - \frac{g_i}{r_i} \exp(-v\tau/r_i) \right) \\ &\times \cos(kv\tau) M_1(k, t - \tau). \end{aligned} \tag{26}$$

In the following, we will discuss the model (24) in the context of a Turing bifurcation [38]. In order to illustrate our main objective, it is sufficient to study a particular parameter set for which the Lyapunov spectrum $\lambda(k)$ exhibits at the critical control parameter γ_c a pair of vanishing Lyapunov exponents $\lambda(k)$ with $k = \pm k_c$ and $k_c > 0$. Figures 3 and 4 show such a spectrum. In line with our general consideration in Sect. 3, we can assume that for $\gamma < \gamma_c$ the system is stable. Due to the linearity of the problem, it is reasonable to assume that the amplitudes $\tilde{u}(k, t)$ are distributed like Gaussian distributions with vanishing mean values and finite variances. For $\gamma \rightarrow \gamma_c$ the variances of the critical Fourier amplitudes $\tilde{u}(\pm k_c, t)$ become infinite, see also Fig. 5. Finally, for γ slightly larger than

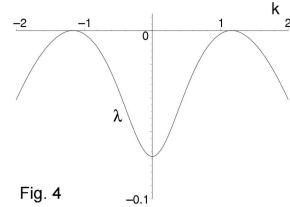
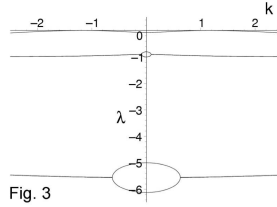


Fig. 3. Real part of the Lyapunov spectrum $\lambda(k)$ at the bifurcation point $\gamma = \gamma_c$ as obtained from Eq. (25) for a particular set of parameters. Critical modes with $\lambda(k) = 0$ occur at $k = \pm k_c$ and $k_c > 0$. Parameters: $g_e = 1.0$, $g_i = 0.2$, $r_e = 0.2$, $r_i = 1.0$, $v = 1.0$, and $\gamma_c = 1.158$.

Fig. 4. Upper band of Fig. 3. The critical modes are at $k = \pm k_c$ and $k_c \approx 1.2$. The homogeneous Fourier mode is stable at the critical point (i.e. $\lambda(0) < 0$).

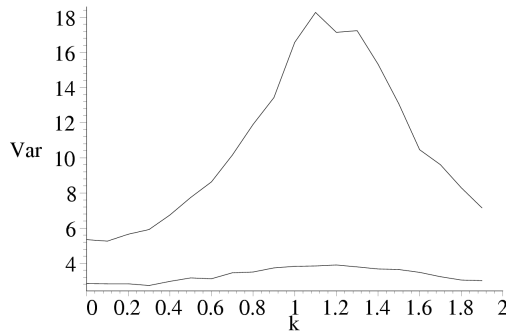


Fig. 5. Variance $\sigma^2(k)$ as obtained by solving Eq. (24) numerically for $\gamma = 1.0$ and $\gamma = 1.1$ (from bottom-up) using an Euler forward scheme [67]. The variance has a maximum at the critical mode $k_c = 1.2$. Other parameters as in Fig. 3.

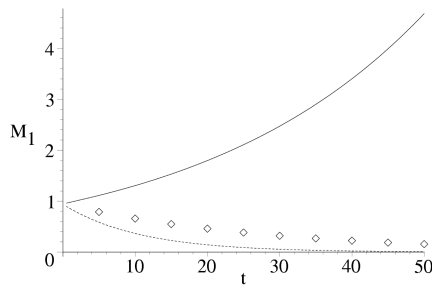


Fig. 6. Evolution of the first moment $M_1(k_c, t)$ of the critical mode with $k_c = 1.2$ computed from Eq. (26) for $\gamma = 1.0 < \gamma_c$ (dashed line) and $\gamma = 1.17 > \gamma_c$ (solid line). For $\gamma = 1.17 > \gamma_c$ the first moment $M_1(0, t)$ of the homogeneous Fourier mode is shown as well (diamonds). The homogeneous Fourier mode is stable, whereas the critical mode is unstable. Other parameters as in Fig. 3.

γ_c the Fourier amplitudes $\tilde{u}(\pm k, t)$ with $k \approx \pm k_c$ become unstable. Since we deal with a Turing bifurcation point at which the imaginary parts of $\lambda(\pm k_c)$ vanish, from Eq. (26) it follows that the first moments $M_1(k, t)$ with $k \approx \pm k_c$ increase monotonically with time, see Fig. 6. In sum, we deal here with the emergence of a Turing pattern in the neural field and with critical fluctuations at the Turing bifurcation point.

5. $1/f^\alpha$ -Fluctuations for specific kernels

Finally, this section discusses the power spectrum of the resulting spatiotemporal field according to the results in Sect. 3. The assumed connectivity is local and excitatory with $K(x) = K_e(x)$ taken from Sect. 4.1, it is $v = v_e$ and the re-scaled temporal operator $\hat{L}_t = \partial/\partial t + 1$ is applied. In addition, we recall the coarse-graining of the neural field. Let the diameter of the smallest spatial element, i.e. the macrocolumn, be Δx , then there is a maximum spatial frequency $k_{\max} = 2\pi/\Delta x$. That is only spatial modes on larger spatial scales than Δx contribute to the spatiotemporal activity.

5.1. Infinite transmission speed

In a first analysis step, the delay by axonal transmission is negligible, i.e. $v \rightarrow \infty$. Then the quantities in Eq. (13) read $m = 1$, $r = 1$ and

$$\Omega(k) = -i \left(1 - \frac{g\gamma}{1 + Dk^2 + 1} \right), \quad P(k) = \frac{1 + Dk^2}{2[g\gamma - (1 + Dk^2)]}.$$

Recalling the relation $\lambda(k) = -i\Omega(k)$, the maximum time scale $1/\lambda(k)$ occurs at $k = 0$ with $\lambda(0) = -(1 - \gamma g)$. That is $\gamma_c = 1/g$ represents the critical control parameter and $\lambda(k) < 0 \forall k, \gamma < \gamma_c$. The power spectrum reads

$$S^2(\omega) = \frac{2Q}{(2\pi)^{3/2}\sqrt{D}} \int_{-k_0}^{k_0} \frac{(u^2 + 1)^2}{\omega^2(u^2 + 1)^2 + (u^2 + 1 - g\gamma)^2} du \tag{27}$$

with $k_0 = k_{\max}\sqrt{D} = 2\pi\sqrt{D}/\Delta x$. That is the power spectrum depends only on the ratio of the spatial interaction scale \sqrt{D} to the diameter of the ensemble entity Δx . Figure 7 shows the power spectrum for several control parameters and fixed ratio $\sqrt{D}/\Delta x$. For $\omega > 1$, the plot reveals Brownian fluctuations with $S^2(\omega) \sim 1/\omega^2$ for all control parameters. In contrast, for $\omega < 1$ the plot reveals white noise activity with $S^2(\omega) \sim \text{const}$ far from the stability threshold, i.e. $\gamma \ll \gamma_c$, while $1/f^\alpha$ with $0 < \alpha < 2$ activity occurs near the stability threshold. In more detail, in the case of $\gamma = 0.95/g$ the spectrum exhibits $S^2(\omega) \sim 1/\omega^{0.15}$ with $0.02 < \omega < 0.2$, while $\gamma = 0.99/g$ yields the rough approximation $S^2(\omega) \sim 1/\omega^{0.37}$ in the frequency range $0.003 < \omega < 0.8$. Hence, $1/f^\alpha$ -activity occurs near the stability threshold only and α increases with increasing control parameter γ .

In addition, the corresponding autocorrelation functions (12) reveals further information on the resulting time scales and we obtain from Eq. (12)

$$C(\tau) = \frac{Q}{2\pi\sqrt{D}} \int_{-k_0}^{k_0} \frac{1 + u^2}{g\gamma - 1 - u^2} \exp((g\gamma - 1 - u^2)/(1 + u^2)\tau) du.$$

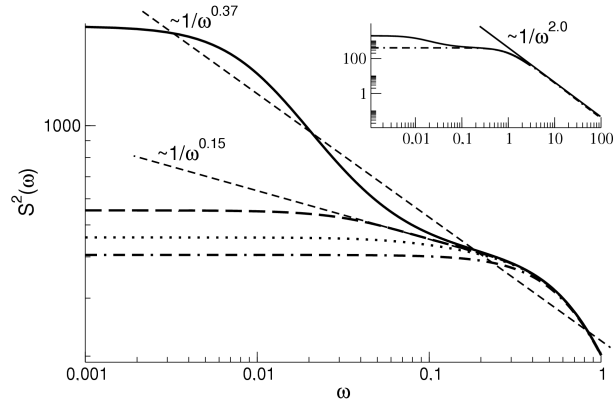


Fig. 7. The log-log-plot of the power spectrum from Eq. (27) for various control parameters γ and infinite transmission speed. The inset shows the log-log-plot of the power spectrum for a wider frequency range and the lowest and highest control parameter corresponding to the line style encoding. The different line types represent $\gamma = 0.99\gamma_c$ (solid line), $\gamma = 0.95\gamma_c$ (dashed line), $\gamma = 0.9\gamma_c$ (dotted line) and $\gamma = 0.5\gamma_c$ (dotted-dashed line). Further parameters are $k_0 = 200$, i.e. $\Delta x \approx \sqrt{D}/32$, and $2Q/((2\pi)^{3/2}\sqrt{D}) = 1.0$.

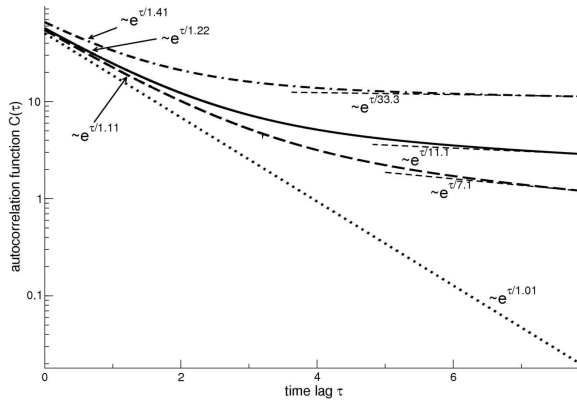


Fig. 8. The log-plot of the autocorrelation function $C(|t-t'|) = C(\tau)$ from Eq. (12) for various control parameters γ and infinite transmission speed. The different line types represent $\gamma = 0.99\gamma_c$ (dotted-dashed line), $\gamma = 0.95\gamma_c$ (solid line), $\gamma = 0.9\gamma_c$ (dashed line) and $\gamma = 0.1\gamma_c$ (dotted line). Further parameters are $k_0 = 200$, i.e. $\Delta x \approx \sqrt{D}/32$, and $2Q/((2\pi)^{3/2}\sqrt{D}) = 1.0$.

Figure 8 shows $C(\tau)$ for various control parameters. Far from threshold the fluctuations evolve on a single time scale τ_0 with $C(\tau) \sim \exp(-\tau/\tau_0)$, while approaching the stability threshold $\gamma \rightarrow \gamma_c$ the underlying time scales separate into short-term scales, i.e. $\tau \rightarrow 0$, and long-term scales with $\tau \rightarrow \infty$. That is long-term memory effects occur near the threshold. Furthermore, the increase in the control parameter increases both the short-term and long-term correlation times. In this

context, we mention the similarity to the results of a recent work [76] revealing the prebifurcation rise in correlation time near the bifurcation threshold in a noisy nonlinear map.

A further study on the impact of the ratio $\sqrt{D}/\Delta x$ to the spectral properties reveals a decreasing exponent α while increasing this ratio for $\omega < 1$ (Fig. 9). That is long-range (short-range) interactions yield low (high) values of α . In addition, the plotted spectra exhibit the same slope for $\omega > 1$, Brownian activity is retained for large frequencies.

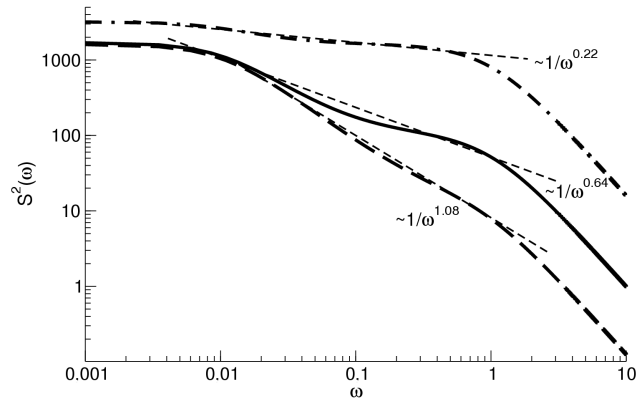


Fig. 9. The log-log-plot of the power spectrum from Eq. (27) for various ratios $\sqrt{D}/\Delta x$ and infinite transmission speed. The different line types represent $\sqrt{D} = 128\Delta x$ (dotted-dashed line), $\sqrt{D} = 8\Delta x$ (solid line) and $\sqrt{D} = \Delta x/2$ (dashed line). Further parameters are $\gamma = 0.99\gamma_c$ and $Q/(2\pi\sqrt{2\pi D}) = 1.0$.

Essentially in the case of negligible spatial interaction $\sqrt{D}/\Delta x \rightarrow 0$, the spectrum approaches the Lorentz-function

$$S^2(\omega) = \frac{2Qk_0}{\pi\sqrt{2\pi}} \frac{1}{\omega^2 + (1 - g\gamma)^2}. \quad (28)$$

It is well known [77] that such a Lorentz-spectrum reflects a relaxation process at time scale $1/(1 - g\gamma)$. That is negligible spatial interaction yields relaxation on a single time scale. This behaviour is reasonable, as $\sqrt{D}/\Delta x \rightarrow 0$ yields the spatial decoupling of the neural field into local elements. Since the applied external noise does not introduce spatial correlations (cf. Sect. 3) either, each element of the neural field responds to the applied external noise by relaxation on the same time scale. Hence, $1/f^\alpha$ may occur for spatially coupled fields only. This finding is in accordance with previous models on power spectra at anesthetic-induced first-order phase transitions [26]. That model neglects spatial interactions and exhibits $S^2(\omega) \sim 1/\omega^2$ at the transition threshold, i.e. no $1/f^\alpha$ -activity.

5.2. Finite transmission speed

Now, we examine how finite transmission speeds affect the power spectrum. In the case of large transmission speeds $v \gg \omega$ utilizing Eq. (11) yields $m = 1$, $r = 1$,

$$\Omega(k) = i(1 + Dk^2) \frac{\gamma g - (1 + Dk^2)}{(1 + Dk^2)^2 + (1 - Dk^2)g\gamma\sqrt{D}/v},$$

$$P(k) = -\frac{(1 + Dk^2)^2 + (1 - Dk^2)g\gamma/v}{2(1 + Dk^2)(g\gamma - 1 - Dk^2)},$$

and the power spectrum

$$S^2(\omega) = \frac{2Q}{(2\pi)^{3/2}\sqrt{D}} \times \int_{-k_0}^{k_0} \frac{[(u^2 + 1)^2 + g\gamma T(1 - u^2)]^2}{\omega^2 [(u^2 + 1)^2 + g\gamma T(1 - u^2)]^2 + (1 + u^2)^2(u^2 + 1 - g\gamma)^2} du \quad (29)$$

with $T = \sqrt{D}/v$. We remark that T may be interpreted as the interaction time of spatial connections. Further $v \rightarrow \infty$ yields vanishing interaction time $T \rightarrow 0$ and Eq. (29) casts to Eq. (27).

In the case of $T < 2/\gamma g$ and $\gamma g < 1$ it is $-1 < \lambda(k) < 0$, i.e. temporal stability. For these parameter ranges the largest time scale occurs at $k = 0$ with $1/\lambda(0) = 1/\bar{v}(1 - 1/\gamma g)$ and thus the critical control parameter is $\gamma_c = 1/g$. That

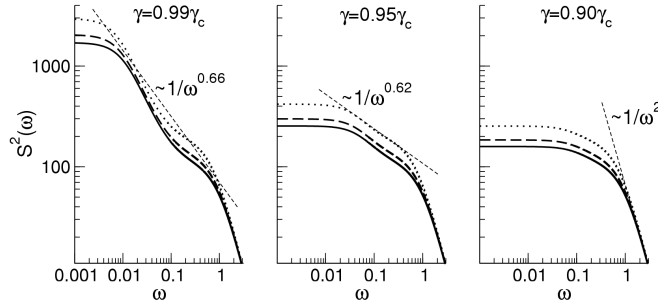


Fig. 10. The log-log-plots of the power spectrum from Eq. (29) for various control parameters γ and finite transmission speeds, i.e. non-vanishing spatial interaction times T . The left panel shows a linear estimation of $\log_{10} S^2(\omega)$ for intermediate frequencies and $T = 0.33$ by a dashed line. The estimated value $\alpha = 0.66$ is valid for all three values of T . Similarly, the value $\alpha = 0.62$ in the center part is valid for all T . Both latter parts show white noise activity and Brownian activity for $\omega \rightarrow 0$ and $\omega > 1$, respectively. In contrast, the right part does not exhibit frequency ranges with $0 < \alpha < 2$ and shows white noise activity and Brownian activity only. The different line types represent the interaction times $T = 0.33$ (dotted line), $T = 0.10$ (dashed line) and $T = 0.001$ (solid line). Parameters are chosen to $k_0 = 2\pi \cdot 16$ and $2Q/((2\pi)^{3/2}\sqrt{D}) = 1.0$.

is $\gamma < \gamma_c$ ensures the temporal stability of the field dynamics. Figure 10 shows the power spectra for various control parameters and values of T . Similar to the previous section, $1/f^\alpha$ -activity occurs near the threshold $\gamma \approx \gamma_c$ only in contrast to the case of lower control parameters $\gamma < \gamma_c$. Further, it turns out that increasing T over a large range with fixed γ increases the overall power of the field but does not change the values of α . Summarizing, at control parameters $\gamma < \gamma_c$ large transmission speeds, i.e. small spatial interaction times, may change the overall spectral power but do not affect the value of α .

6. Discussion

The previous sections discuss the stability and stochastic properties of evoked neural activity. First we show that the transmission delay in the spatial domain reduces to a distribution of constant delays in the corresponding Fourier domain. Hence, the linear neural field evolves in Fourier-space according to affine delay differential equations. Further investigations on the evoked response to external stimulation reveal that only the characteristic roots of the delay differential equations determine the field stability. In addition, the temporal spectrum of the evoked activity turns out to depend mainly on the distribution of the spatial synaptic connectivities and the synaptic delay. These findings are valid for general connectivity kernels. In order to learn more about the evoked response to random fluctuations, we discuss the stability and temporal power spectrum in the case of specific synaptic connectivities. In a first example, it is shown that short-range excitation is equivalent to diffusive interaction. An additional discrete inhibitory interaction yields a Hopf-bifurcation for the spatially constant mode. We derive the variance of the stationary activity distribution for all Fourier modes and find a divergent fluctuation variance at the bifurcation threshold of the constant mode. That is critical fluctuations occur at the oscillatory bifurcation threshold. Similar constant oscillations have been found in deterministic neural networks [78], while the critical fluctuations have been found experimentally in oscillatory neural activity [22]. In a further discussion, we examine neural fields with local excitation and lateral inhibition and find critical fluctuations at the threshold of a Turing bifurcation.

Eventually, the final section focus to $1/f^\alpha$ -activity in purely diffusive neural fields. The evoked power spectrum reveals $1/f^\alpha$ -fluctuations for small frequencies near the bifurcation threshold, while for large frequencies the power spectrum shows $1/f^2$ -activity reflecting Brownian motion dynamics. These findings reveal the presence of both, a short-term and a long-term correlation time, that is long-term memory effects near the stability threshold. Remarkably the spectral properties are different far from the bifurcation threshold, where the power spectrum shows similarity to the Lorentz-spectrum indicating a single relaxation process. That is the fluctuations exhibit white noise behaviour for small frequencies and Brownian motion properties for large frequencies. In addition, all these findings are retained for both infinite and large finite transmission speeds.

Several studies pointed out that $1/f^\alpha$ -fluctuations occur in the case of multiple time scales. The present work confirms this finding. However, in our neural model the multiple time scales originate from the multiple spatial scales. In addition, these $1/f^\alpha$ -fluctuations occur near the bifurcation threshold only, though the neural system exhibits multiple time scales for a large range of control parameters. Hence, this finding fosters the hypothesis of necessary criticality in a system for the occurrence of $1/f^\alpha$ -activity (cf. [21]). Further the successful modelling of critical fluctuations in the presence of transmission delay in nonlocal neural models is in accordance with experimental findings [10] and thus supports our mesoscopic model based on neural populations. The fact that our rather simple neural model explains $1/f^\alpha$ -activity in neural activity and indicates its necessary neural mechanism, namely spatial coupling. Future work may include further important neural mechanisms as inclusion of spike-timing effects [56, 58], temporal feedback delay present in the thalamocortical system and the temporal adaptation of synaptic strength, i.e. inclusion of plasticity effects.

Acknowledgments

A. Hutt has been supported by the DFG research center *Mathematics for Key Technologies (Matheon)* in Berlin, Germany.

References

- [1] H. Haken, *Synergetics: Introduction and Advanced Topics*, Springer, Berlin 2004.
- [2] A. Nitzan, P. Ortoleva, J. Deutch, J. Ross, *J. Chem. Phys.* **61**, 1056 (1974).
- [3] Y. Kuramoto, *Chemical Oscillations, Waves, and Turbulence*, Dover, Mineola 2003.
- [4] C.W. Gardiner, *Handbook of Stochastic Methods*, Springer, Berlin 1983.
- [5] B. Lindner, J. Garcia-Ojalvo, A. Neiman, L. Schimansky-Geier, *Phys. Rep.* **392**, 321 (2004).
- [6] W. Horsthemke, R. Lefever, *Noise-Induced Transitions: Theory and Applications in Physics, Chemistry, and Biology*, Springer, Berlin 1984.
- [7] D. Paré, E. Shink, H. Gaudreau, A. Destexhe, E.J. Lang, *J. Neurophysiol.* **79**, 1450 (1998).
- [8] L.G. Nowak, M.V. Sanchez-Vives, D.A. McCormick, *Cerebral Cortex* **7**, 487 (1997).
- [9] M. Usher, M. Stemmler, *Phys. Rev. Lett.* **74**, 326 (1995).
- [10] Y. Chen, M. Ding, J.A.S. Kelso, *Phys. Rev. Lett.* **79**, 4501 (1997).
- [11] N. Ho, A. Destexhe, *J. Neurophysiol.* **84**, 1488 (2000).
- [12] D. Nozaki, J.J. Collins, Y. Yamamoto, *Phys. Rev. E* **60**, 4637 (1999).
- [13] M. Rudolph, A. Destexhe, *Phys. Rev. Lett.* **86**, 3662 (2001).
- [14] F. Liu, B. Hu, W. Wang, *Phys. Rev. E* **63**, 031907 (2001).
- [15] P. beim Graben, J. Kurths, *Phys. Rev. Lett.* **90**, 100602 (2003).

- [16] P. Dutta, P.M. Horn, *Rev. Mod. Phys.* **53**, 497 (1981).
- [17] Th.F. Nonnenmacher, R. Metzler, in: *Applications of Fractional Calculus in Physics*, Ed. R. Hilfer, World Scientific, Singapore 2000.
- [18] J. Bernamont, *Ann. Phys. (Leipzig)* **7**, 71 (1937).
- [19] E. Milotti, *Phys. Rev. E* **51**, 3087 (1995).
- [20] B. Kaulakys, T. Meskauskas, *Phys. Rev. E* **58**, 7013 (1998).
- [21] P. Bak, C. Tang, K. Wiesenfeld, *Phys. Rev. Lett.* **59**, 381 (1987).
- [22] G.V. Wallenstein, J.A.S. Kelso, S.L. Bressler, *Physica D* **84**, 626 (1995).
- [23] V.K. Jirsa, H. Haken, *Phys. Rev. Lett.* **7**, 960 (1996).
- [24] T.D. Frank, A. Daffertshofer, P.J. Beek, H. Haken, *Physica D* **127**, 233 (1999).
- [25] T.D. Frank, A. Daffertshofer, C.E. Peper, P.J. Beek, H. Haken, *Physica D* **144**, 62 (2000).
- [26] M.L. Steyn-Ross, D.A. Steyn-Ross, *Phys. Rev. E* **60**, 7299 (1999).
- [27] P. Tass, *Phase Resetting in Medicine and Biology*, Springer, Berlin 1999.
- [28] F.H. Lopes da Silva, W. Blanes, S.N. Kalitzin, J. Parra, P. Suffczynski, D.N. Velis, *Epilepsia* **44**, (Suppl. 12), 72 (2003).
- [29] D.J. Pinto, G.B. Ermentrout, *SIAM J. Appl. Math.* **62**, 206 (2001).
- [30] J.R. Brasic, *Percep. Motor Skills* **86**, 851 (1998).
- [31] S.H. Isaacson, J. Carr, A.J. Rowan, *Neurol.* **43**, 1619 (1993).
- [32] G.B. Ermentrout, J.D. Cowan, *Biol. Cybern.* **34**, 137 (1979).
- [33] P. Tass, *J. Biol. Phys.* **23**, 21 (1997).
- [34] D. Golomb, G.B. Ermentrout, *Network: Comput. Neural Syst.* **11**, 221 (2000).
- [35] V.K. Jirsa, M.Z. Ding, *Phys. Rev. Lett.* **93**, 070602 (2004).
- [36] H. Haken, *Europ. Phys. J. B* **18**, 545 (2000).
- [37] P.L. Nunez, *Neocortical Dynamics and Human EEG Rhythms*, Oxford University Press, New York 1995.
- [38] A. Hutt, M. Bestehorn, T. Wennekers, *Network: Comput. Neural Syst.* **14**, 351 (2003).
- [39] F.M. Atay, A. Hutt, *SIAM J. Appl. Math.* **65**, 644 (2005).
- [40] S.M. Crook, G.B. Ermentrout, M.C. Vanier, J.M. Bower, *J. Comput. Neurosci.* **4**, 161 (1997).
- [41] S. Coombes, G.J. Lord, M.R. Owen, *Physica D* **178**, 219 (2003).
- [42] P.A. Robinson, C.J. Rennie, J.J. Wright, *Phys. Rev. E* **56**, 826 (1997).
- [43] P.A. Robinson, P.N. Loxley, S.C. O'Connor, C.J. Rennie, *Phys. Rev. E* **63**, 041909 (2001).
- [44] C.J. Rennie, P.A. Robinson, J.J. Wright, *Biol. Cybern.* **86**, 457 (2002).
- [45] J.J. Wright, D.T.J. Liley, *Biosystems* **63**, 15 (2001).
- [46] J.J. Wright, *Biol. Cybern.* **81**, 131 (1999).
- [47] D.H. Hubel, T.N. Wiesel, *J. Physiol.* **26**, 994 (1963).

- [48] J.B. Levitt, D.A. Lewis, T. Yoshioka, J.S. Lund, *J. Comp. Neurol.* **338**, 360 (1993).
- [49] O. Lejeune, M. Tlidi, R. Lefever, *Int. J. Quantum Chem.* **98**, 261 (2004).
- [50] P.C. Bressloff, J.D. Cowan, M. Golubitsky, P.J. Thomas, M.C. Wiener, *Neural Computation* **14**, 473 (2002).
- [51] T.D. Frank, P.J. Beek, *Phys. Rev. E* **64**, 021917 (2001).
- [52] T.D. Frank, P.J. Beek, R. Friedrich, *Phys. Rev. E* **68**, 021912 (2003).
- [53] H.R. Wilson, J.D. Cowan, *Kybernetik* **13**, 55 (1973).
- [54] V.K. Jirsa, *Neuroinformatics* **2**, 183 (2004).
- [55] W.J. Freeman, *Neurodynamics: An Exploration in Mesoscopic Brain Dynamics (Perspectives in Neural Computing)*, Springer-Verlag, Berlin 2000.
- [56] W.M. Kistler, R. Seitz, J.L. van Hemmen, *Physica D* **114**, 273 (1998).
- [57] S. Amari, *Biol. Cybern.* **27**, 77 (1977).
- [58] W. Gerstner, *Phys. Rev. E* **51**, 738 (1995).
- [59] G.B. Ermentrout, J.D. Cowan, *SIAM J. Appl. Math.* **38**, 1 (1980).
- [60] P.C. Bressloff, S. Coombes, *Inter. J. Mod. Phys. B* **11**, 2343 (1997).
- [61] H.R. Wilson, J.D. Cowan, *Biophys. J.* **12**, 1 (1972).
- [62] W.J. Freeman, *Int. J. Bif. Chaos* **2**, 451 (1992).
- [63] M. Steriade, D.A. McCormick, T.J. Sejnowski, *Science* **262**, 679 (1993).
- [64] J. Cowan, G. Ermentrout, in: *Studies in Mathematical Biology, Part I: Cellular Behavior and the Development of Pattern*, Ed. S. Levin, MAA, Washington (DC) 1978, p. 67.
- [65] J.K. Hale, S.M.V. Lunel, *Introduction to Functional Differential Equations*, Springer, Berlin 1993.
- [66] A.A. Gushchin, U. Kuechler, *Stochastic Proc. Appl.* **88**, 195 (2000).
- [67] H. Risken, *The Fokker–Planck equation — Methods of Solution and Applications*, Springer, Berlin 1989.
- [68] M. Steriade, E.G Jones, R.R. Llinas, *Thalamic Oscillations and Signalling*, Wiley, New York 1990.
- [69] R.D. Driver, *Ordinary and Delay Differential Equations — Applied Mathematical Sciences*, Vol. 20, Springer, New York 1977.
- [70] U. Küchler, B. Mensch, *Stoch. Stoch. Rep.* **40**, 23 (1992).
- [71] M.C. Mackey, I.G. Nechaeva, *Phys. Rev. E* **52**, 3366 (1995).
- [72] A.A. Budini, M.O. Caceres, *Phys. Rev. E* **70**, 046104 (2004).
- [73] T.D. Frank, *Phys. Rev. E* **69**, 061104 (2004).
- [74] R. Ben-Yishai, R.L. Bar-Or, H. Sompolinsky, *Proc. Natl. Acad. Sci.* **92**, 3844 (1995).
- [75] T. Wennekers, *Neural Computation* **13**, 1721 (2001).
- [76] E.D. Surovyatkina, *Phys. Lett. A* **329**, 169 (2004).
- [77] W. Schottky, *Phys. Rev.* **28**, 74 (1926).
- [78] M.G. Earl, S.H. Strogatz, *Phys. Rev. E* **67**, 036204 (2003).